Electronic Supplementary Material (ESI) for Nanoscale.

Supplementary information for

Vacancy-driven phase transition in MoX_2 (X: S, Se and Te) nanoscrolls

Methods

Materials

$MoTe_2$ powder (<10 μm) was purchased from Materion. $MoSe_2$ (-325 mesh) and MoS_2 (<2 μm) powder, lithocholic acid (>97 %), and *o*-dichlorobenzene (anhydrous) were purchased from Sigma-Aldrich. All chemical reagents were of analytical grades.

Preparation of the dispersed MoS_2 and $MoSe_2$ solutions

The dispersed MoS_2 and $MoSe_2$ were prepared according to previous work[1]; MoS_2 (1.5g) and $MoSe_2$ (1.5g) were added to 300mL *o*-dichlorobenzene (ODCB), respectively. The mixture was homogenized at 2400 rpm for 1 hr (IKA-RW20, Stage II), followed by cuphorn sonication for 30 minutes (Power%= 50 %, Pulse = 20 sec. (On), 10 sec (Off)). Finally, the slurry was centrifuged at 4400 rpm for 30 minutes. The supernatant was obtained in ODCB.

Preparation of the dispersed $MoTe_2$ solutions

The dispersed $MoTe_2$ solutions were prepared from $MoTe_2$ (<10 μm) utilizing a previous method with slight modification. $MoTe_2$ powder (1.5 g) was added to 300 mL isopropanol. The sealed flask was sonicated for 1 hour and then the dispersion was centrifuged at 4400 rpm for 30 mins to remove aggregates. The supernatant was then obtained.

Synthesis of starting material (*N-(2-aminoethyl)-3α-hydroxy-5β-cholan-24-amide (LCA)*)

LCA was synthesized by the reaction of methyl lithocholate with excess of diaminoethane according to previous work[2]; The methyl lithocholate was dissolved in methanol and excess of diaminoethane (20 - 30 times) was added to the methyl lithocholate solution. The solution

was heated with an oil bath (80 - 90 °C) for 2 days. The resulting solution was poured into the water and the precipitate filtered. The product was recrystallized from acetonitrile and dried in a vacuum.

Synthesis of 1T or 1T' MoX_2 (X; S, Se and Te) nanoscrolls

MoX_2 nanoscrolls were synthesized by the solution process.[1] LCA of 0.02mmol was dissolved in ODCB (1 mL) and heated to 60 °C. Then, the dissolved LCA solution was immediately poured into the dispersed MoX_2 solution (5 ml). The solution with the precipitates was stored at room temperature for 24 hrs. The resulting precipitate was obtained by filtering with a PTFE membrane washed with methanol by centrifugation at 4000 rpm for 20 minutes and followed by decantation. This procedure was repeated at least five times. Thermal treatment was conducted on a hot plate under an argon flow of 100 mL/min. Samples were annealed at a desired temperature for 1 h.

Characterization

A drop of the purified sample by a microsyringe was placed on a holey carbon grid and then methanol was evaporated. HR-TEM measurements were carried out on JEM-2100F with an accelerating voltage of 200 kV. Analysis by Micro-Raman spectrometry (JASCRO NRS-3100) was carried out with an excitation laser of 532nm wavelength using the 100 X objective. Samples were prepared by drop casting of the dispersion on SiO_2/Si substrates and the solvent was evaporated at RT. X-ray Photoelectron Spectroscopy measurements were performed in a type Theta probe base system (Thermo Fisher Scientific Co.). XPS Peak 4.1 was employed to deconvolve the Te 3d and Mo 3d peaks using the Tougaard-type baseline and an iterative least-squared optimization algorithm. Phase transition temperatures (T_p) were

measured by differential scanning calorimetry (DSC) using a SDT Q600 from Auto-DSCQ20 System. The samples were heated from RT to 600^{o}C at heating rate dependence under an argon flow of 100 mL/min. Thermal data acquisition was carried out using a Thermal Analysis software from TA instruments.

Figure S1. TEM images of the dispersed $MoSe_2$ and $MoTe_2$ sheets.

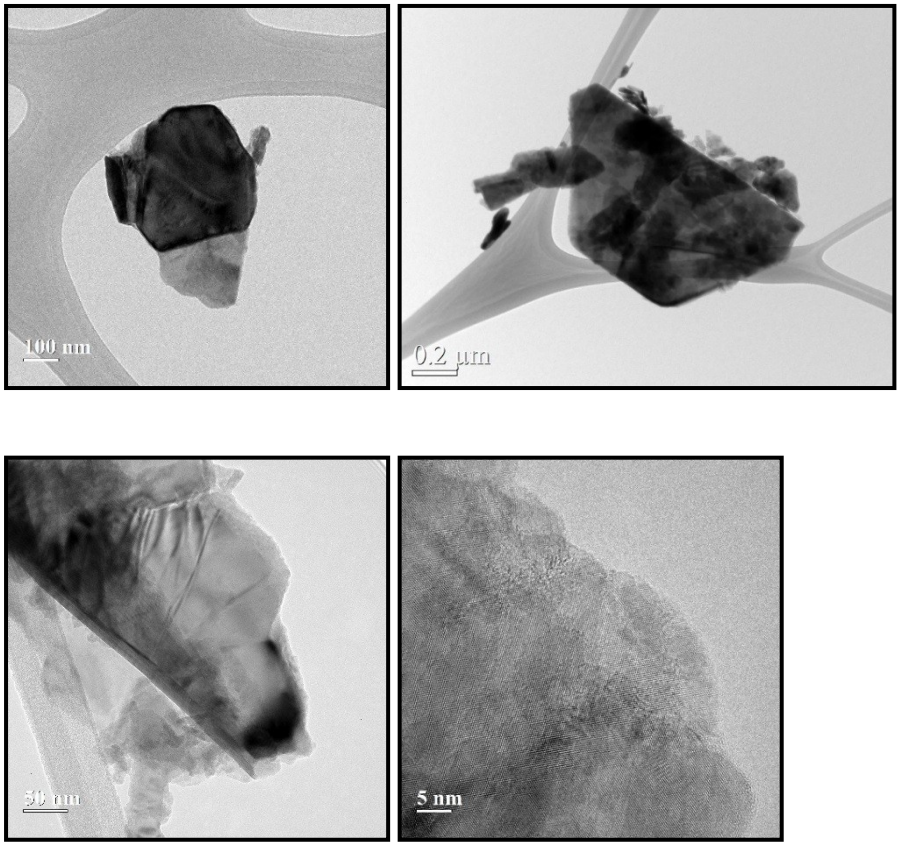

The concentration of the final exfoliated MoX_2 was measured by using the vacuum filter through a weighed membrane. The multi-layer MoX_2 with size of typically several hundred nanometers is observed.

Figure S2. TEM images of 1T@2H MoS_2 scrolls and 1T@2H $MoSe_2$ scrolls at room temperature with a low magnification.

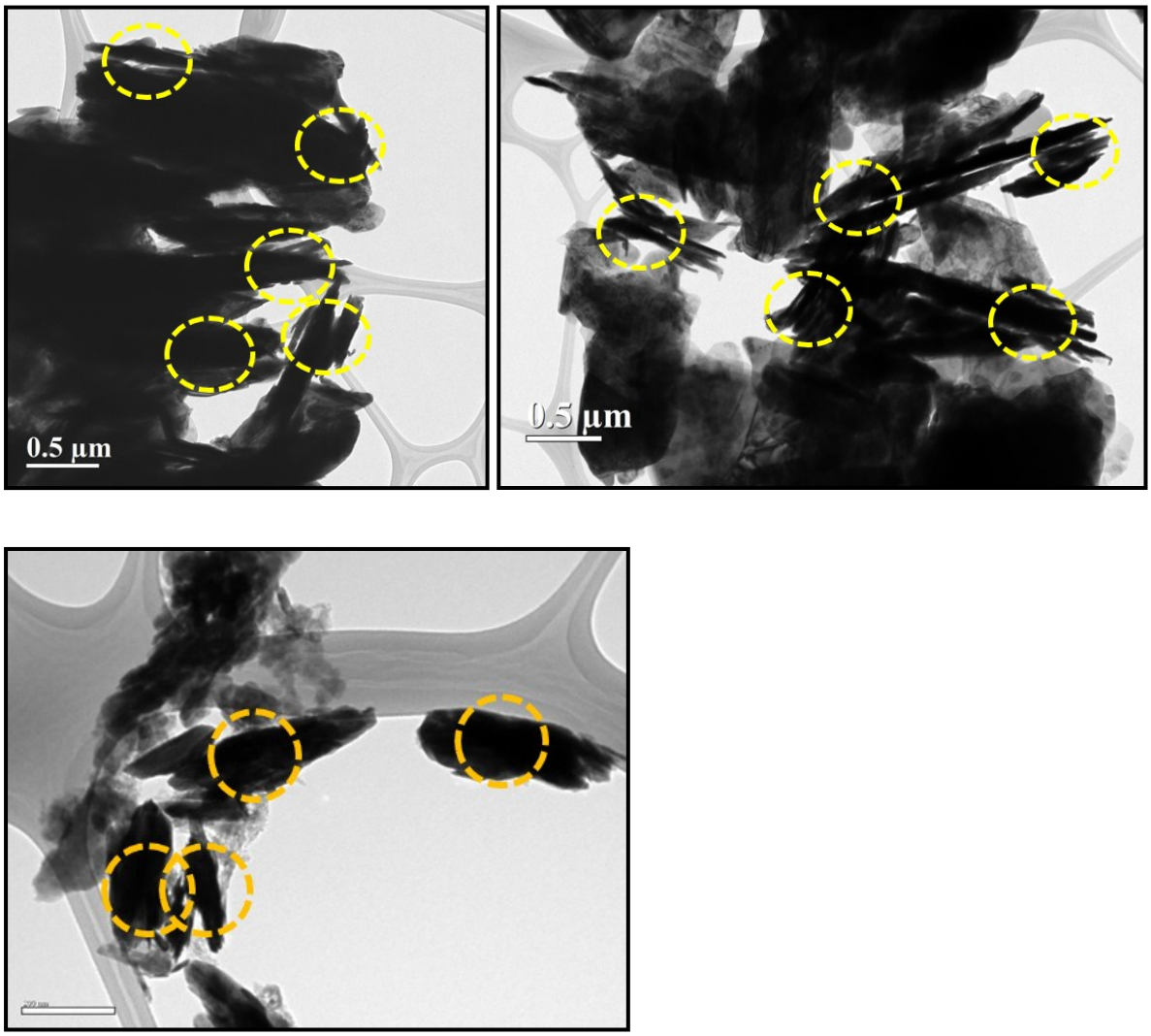

The tube-like morphology scrolled by interaction of MoS_2 and $MoSe_2$ with LCAs, respectively. The TEM images at a low magnification represent the produced 1T@2H MoS_2 scrolls and 1T@2H $MoSe_2$ scrolls.

Figure S3. Collected TEM images 1T@2H MoS_2 scrolls, 1T@2H $MoSe_2$ scrolls and 1T'@2H $MoTe_2$ scrolls from several samples with a diameter from 40 to 100 nm.

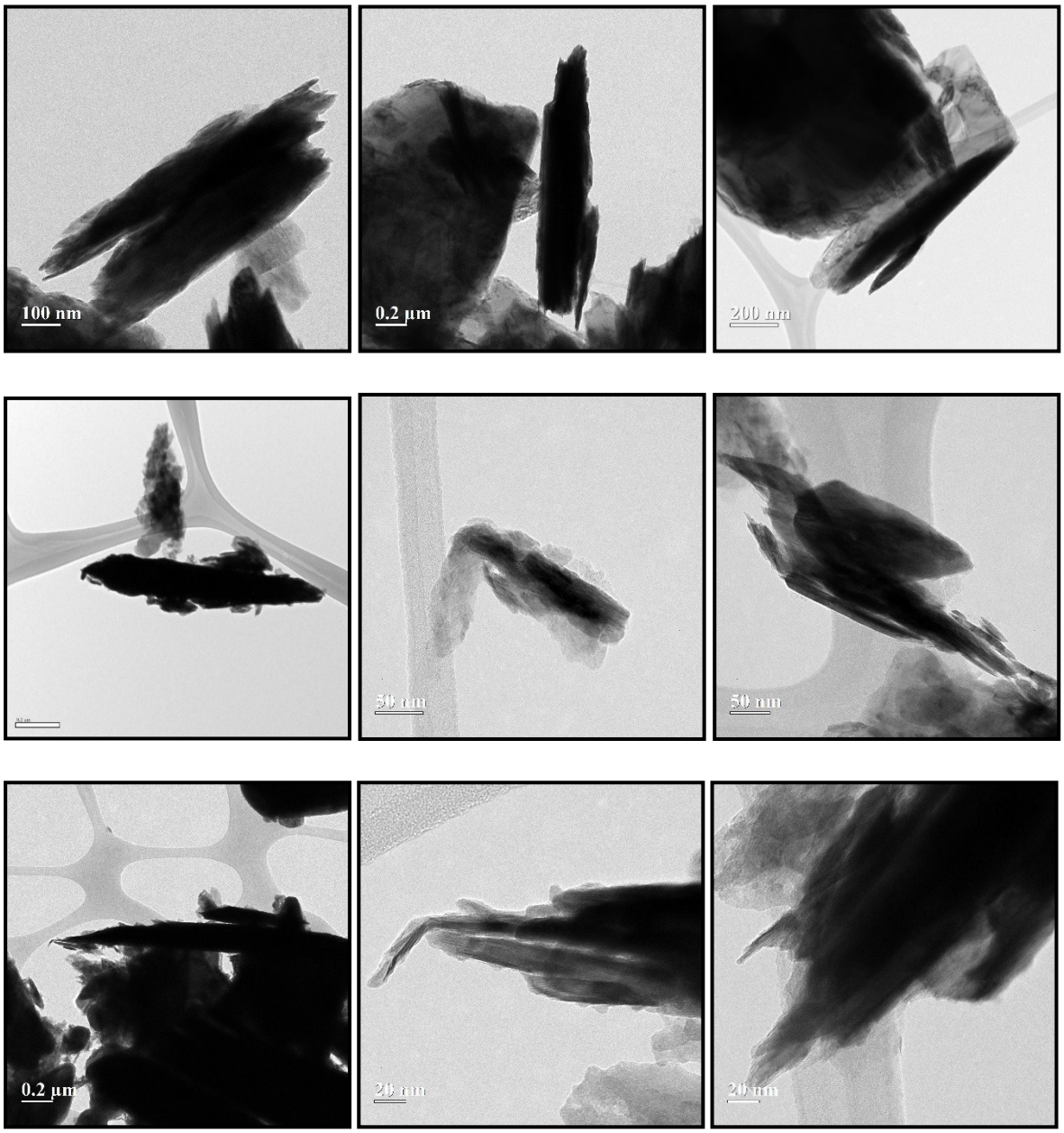

Figure S4. Binding energy measurement for MX_2 (X; S, Se and Te) of 2H, 1T and 1T' phases, respectively.

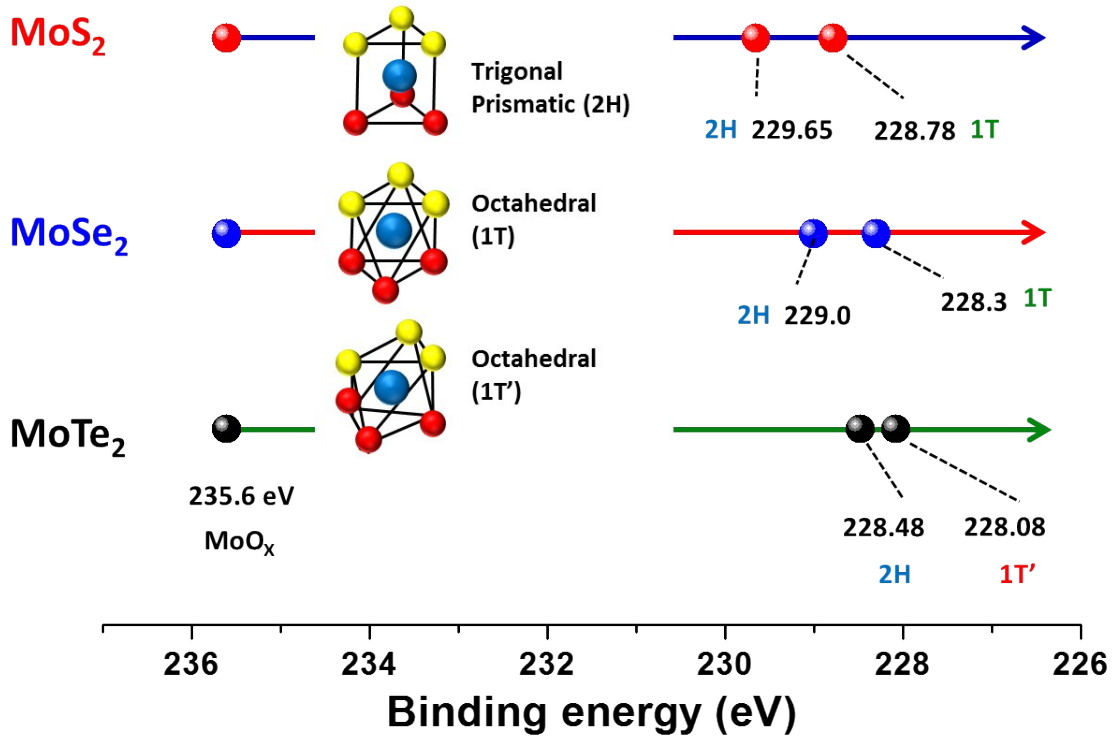

Figure S5. Calculation of the strain energy for 1T@2H MoX_2 nanoscrolls.

We now discuss that the observed behavior can be explained by considering the nanoscrolls induced uniaxial strain on Raman modes responsible for E^1_{2g} and A_{1g}, correspondingly. The uniaxial strain-induced peak splitting for the E^1_{2g} mode enables us to calculate parameters: the Grüneisen parameter, γ, and the shear deformation potential, β, and the solution of the secular equation for the E_{2g} mode $^{\Delta\omega_{E_{2g},1}}$

$$\gamma_{E_{2g}} = -\frac{\Delta\omega_{E_{2g}+} + \Delta\omega_{E_{2g}-}}{2\omega^0{}_{E_{2g}}(1-\nu)\varepsilon} \quad \textbf{(1)}$$

$$\beta_{E_{2g}} = \frac{\Delta\omega_{E_{2g}+} - \Delta\omega_{E_{2g}-}}{\omega^0{}_{E_{2g}}(1+\nu)\varepsilon} \quad \textbf{(2)}$$

$$\Delta\omega^{\pm}{}_{E_{2g}} = -\omega^0{}_{E_{2g}}\gamma_{E_{2g}}(1-\nu)\varepsilon \pm \frac{1}{2}\beta_{E_{2g}}\omega^0{}_{E_{2g}}(1+\nu)\varepsilon \quad \textbf{(3)}$$

where Δω is the change of frequency in the Raman mode, $^{\omega^0{}_{E_{2g}}}$ is the E_{2g} peak position at zero strain, ν is Poisson's ratio and ε is the induced uniaxial tensile strain. The Grüneisen parameter of 1.1 and the shear deformation potential of 0.78 for both monolayer and bilayer MoS_2 attaching to a substrate (ν = 0.33) are reported.[2] In case of formation of 1T@2H MoS_2 scrolls, these calculated parameter is used to estimate the strain applied to free-standing multilayer MoS_2. To insert $^{\omega^0{}_{E_{2g}}}$= 380.9 cm^{-1} from Raman spectra, γ_{E2g} = 1.1, β_{E2g} = 0.78 and Poisson's ratio ν = 0.125 for free-standing MoS_2 in Equation 3,[3] we can obtain the E_{2g} for $\partial\omega_{E_{2g}+}/\partial\varepsilon \sim 2.0$ cm^{-1}/% strain. These results are almost equal to the linear relationship with a slope −1.7 cm^{-1} / % strain obtained by applying uniform tensile strain to few-layer MoS_2.[8] Combining the above results, 1T@2H MoS2 nanoscrolls formed through the rolling 2H MoS_2 sheets can sustain the high local strain greater than ~ 1.7 % compared with that of MoS_2 sheets, which represents the reliable results by virtue of the layer-by-layer Vander Waals interaction energy of overlapping (stability).

Figure S6. Summary the induced strain and vacancy in scrolls obtained from 1T@2H MoS_2 scrolls.

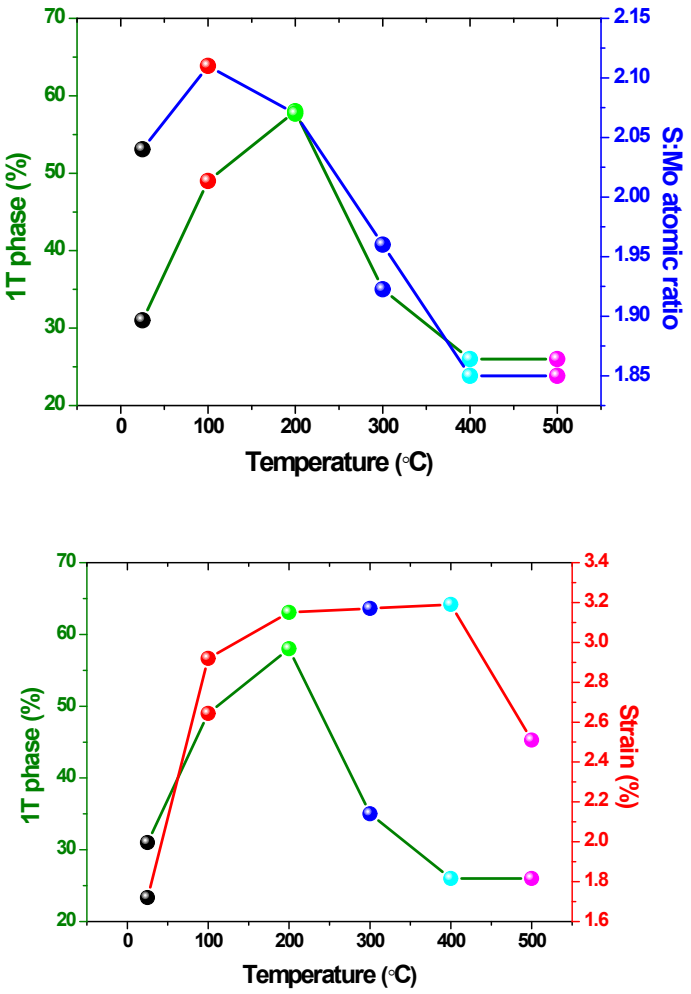

To estimate the applied strains for the temperature dependent 1T@2H MoS2 scrolls, we first consider that the frequency red-shifts of both peaks increase in the range of -3.44, -5.84 and -6.30 cm^{-1} with increasing temperature at 200°C, which converted to the induced uniaxial tensile strain resulting in that of ~ 1.7, 2.9 and 3.2 % for the temperature at 298, 373 and 473K, respectively (which follows a linear relationship with a slope −2.0 cm^{-1} / % strain).[2] When temperature rises further, 1T@2H MoS_2 scrolls may slip on the layer-by-layer S-plane because the tensile strain significantly increases, followed by tensile strain induced vacancy formation, resulting the maximized 1T phases.

Figure S7. The reversible phase transition relation between the 1T metallic phase percentage from XPS spectra of 1T@2H $MoSe_2$ scrolls in different thermal environments (25 < T < 500 °C).

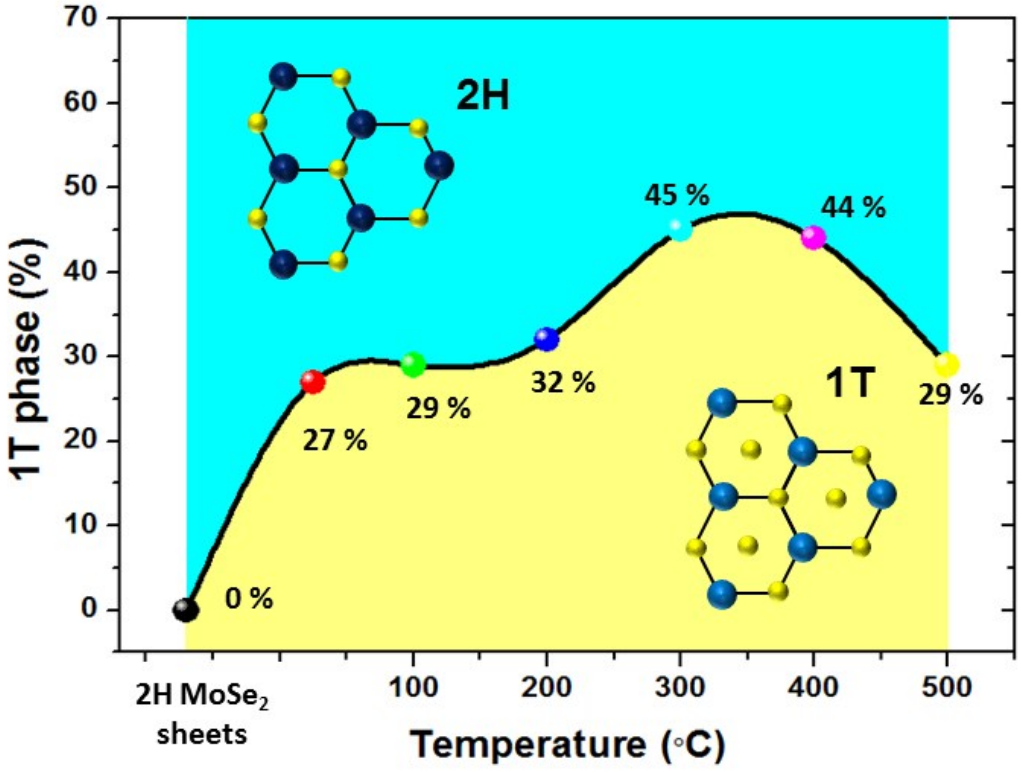

Figure represents the temperature-dependent phase diagram of 1T@2H $MoSe_2$ scrolls for the contents of the 2H and 1T phases. The stable 2H begins to transform into the 1T phase until temperatures rise at 300 °C. The synthesized 1T@2H $MoSe_2$ scrolls that had maximum contents of 1T phase (45 %) at 300 °C were never thermally converted back to the original 2H phase at room temperature.

Figure S8. XPS data for the formation of vacancy in MoX_2 scrolls.

Atom	$MoTe_2$ bulk	$MoTe_2$ sheets	$MoTe_2$ scrolls
Mo	1.00	1.00	1.00
Te	2.00	1.99	**1.89**

Atom	$MoSe_2$ bulk	$MoSe_2$ sheets	$MoSe_2$ scrolls
Mo	1.00	1.00	1.00
Se	2.00	2.00	**1.98**

Atom	MoS_2 bulk	MoS_2 sheets	MoS_2 scrolls
Mo	1.00	1.00	1.00
S	2.00	2.00	**2.04**

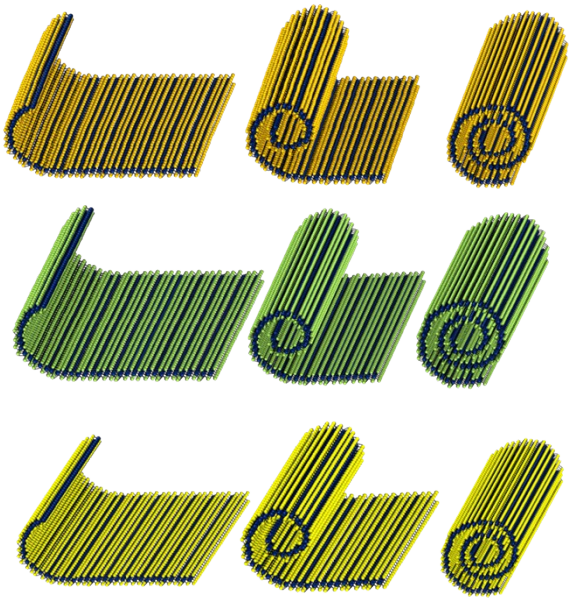

Figure S9. TEM images and Energy dispersive spectrometer (EDS) analysis of 1T'@2H $MoTe_2$ scrolls included by a LCA.

Element	Line Type	k Factor	Absorption Correction	Wt%	Wt% Sigma	Atomic %
C	K series	2.930	1.00	0.40	0.10	**3.42**
O	K series	2.133	1.00	0.41	0.09	**2.67**
Mo	L series	1.894	1.00	51.30	0.36	**55.18**
Te	L series	2.050	1.00	47.89	0.36	**38.73**
Total:				100.00		100.00

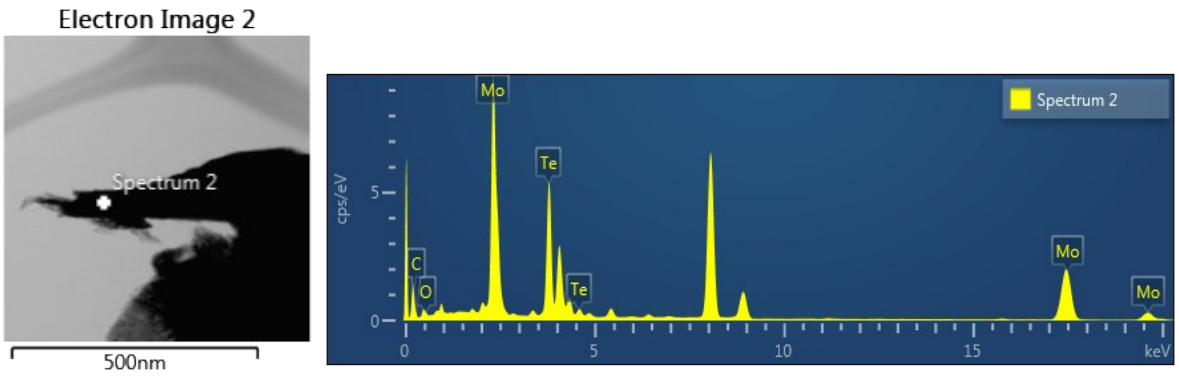

1T'@2H $MoTe_2$ scrolls at the center point were detected by the elementary analysis of Energy dispersive spectrometer (EDS) images. These data show 1T'@2H $MoTe_2$ scrolls containing Te vacancies with corresponding EDS mapping for C, O, Mo and Te.

Figure S10. Thermodynamics of 1T'@2H $MoTe_2$ scrolls. (a) Thermodynamics of 1T'@2H $MoTe_2$ scrolls measured at different heating rates, **(b)** thermodynamics of 1T'@2H $MoTe_2$ scrolls measured from TGA and DSC.

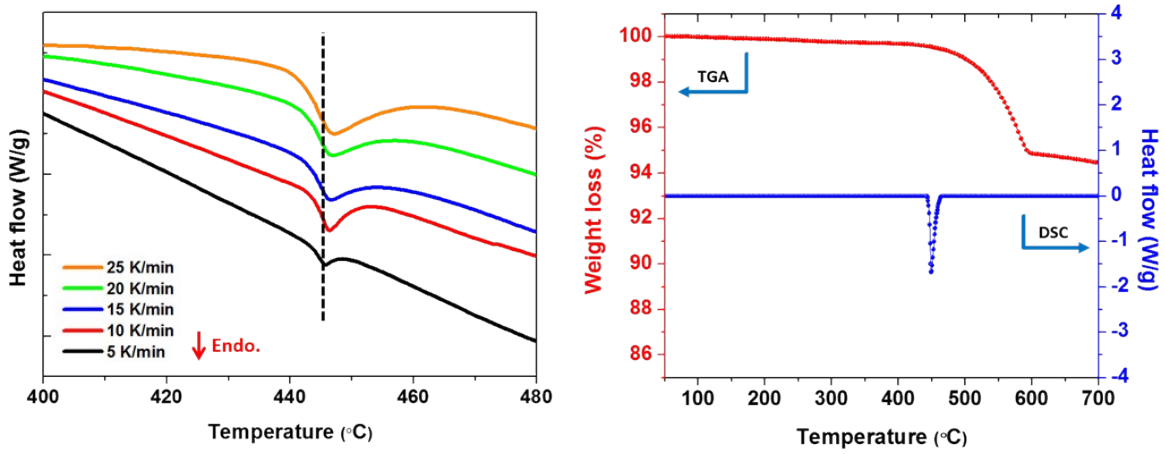

$MoTe_2$ sheets exhibit a temperature-dependent, reversible exothermic phase transition from 2H to 1T' above 820 °C.[3] Therefore, stabilizing the 1T' phase of $MoTe_2$ at room temperature is challenging. As illustrated in **Figure 9a**, 1T'@2H $MoTe_2$ scrolls undergo an irreversible, endothermic phase transition from the stable 2H to the metastable 1T' phase at 446 °C (at a heating rate of 10 K/min), a different phenomenon compared to that observed in the $MoTe_2$ sheets. As illustrated in **Figure 9b**, the thermal gravimetric analysis (TGA) curve does not show any noticeable weight loss at the phase transition temperature. Repeated scans of differential scanning calorimetry (DSC) also did not show any change in the heat absorbed or released, indicating that the phase transition was irreversible.

Figure S11. Electrochemical effects of the 2H MoS_2 nanosheets and their nanoscrolls on the HER activity. Current density at -0.3V vs RHE for 2H MoS_2 (blue curve) sheets and 1T@2H MNSs (red curve) and comparison of Tafel plots from the polarization curves.

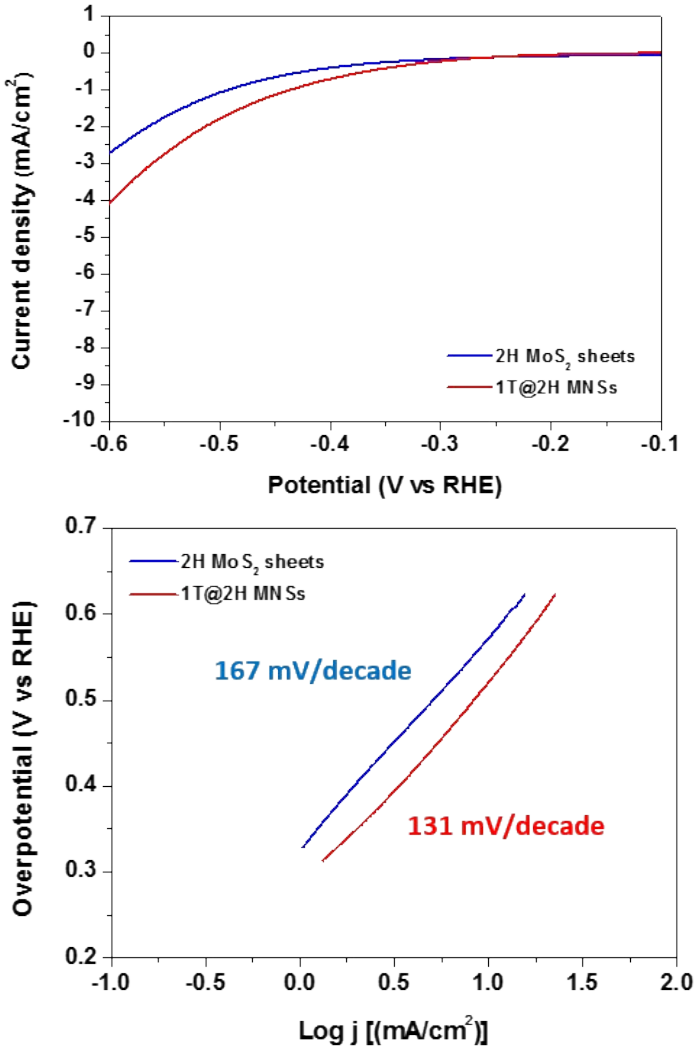

References

1. D. Y. Hwang, K. H. Choi, J. E. Park and D. H. Suh, *Nanoscale*, 2017, **9**, 503-508.
2. M. Löfman, J. Koivukorpi, V. Noponen, H. Salo and E. Sievänen, *Journal of Colloid and Interface Science*, 2011, **360**, 633-644.
3. Mohiuddin, T. M. G. *et al.* Uniaxial strain in graphene by Raman spectroscopy: G peak splitting, Gruneisen parameters, and sample orientation. *Physical Review B* **79**, 205433 (2009).
4. Conley, H. J. *et al.* Bandgap Engineering of Strained Monolayer and Bilayer MoS2. *Nano Letters* **13**, 3626-3630, doi:10.1021/nl4014748 (2013).
5. Castellanos-Gomez, A. *et al.* Local Strain Engineering in Atomically Thin MoS2. *Nano Letters* **13**, 5361-5366, doi:10.1021/nl402875m (2013).